




Polarization dependence of ZnO Schottky barriers revealed by photoelectron spectroscopy

Philipp Wendel , Shanmugapriya Periyannan, Wolfram Jaegermann, and Andreas Klein ^{*}
Technische Universität Darmstadt, Institute of Materials Science, 64287 Darmstadt, Germany

 (Received 27 June 2020; accepted 11 August 2020; published 31 August 2020)

In order to answer the question of whether Schottky barriers on polar ZnO surfaces are different at Zn- and O-terminated surfaces, the interface formation of *n*-type ZnO and different high work function metals and metal oxides (Pt, PtO_x, and RuO₂) with Schottky barrier heights of up to 1.5 eV has been studied using photoelectron spectroscopy with *in situ* sample preparation. The experiments are designed to exclude the effects of substrate reduction and consequent Fermi level pinning by high concentrations of oxygen vacancies. Moreover, by including the Zn LMM Auger emission in the analysis, it is demonstrated that an accurate extraction of barrier heights needs to take into account that the screening of the photoelectron core hole can change in the course of contact formation. The polarization dependence of Schottky barriers, which is important for piezotronic applications, is in most cases dominated by the influence of defects. Reducing the influence of defects, up to ~240 meV higher Schottky barriers are revealed on oxygen-terminated surfaces. This is opposite to what has been reported in the literature but agrees with the dependence of barrier heights expected for an incomplete screening of the polarization of ZnO by the electrode as for ferroelectric materials.

DOI: [10.1103/PhysRevMaterials.4.084604](https://doi.org/10.1103/PhysRevMaterials.4.084604)

I. INTRODUCTION

ZnO is intensively studied due to its diverse properties finding application as transparent conductive electrodes in thin film solar cells [1], in the field of piezotronics [2–4], as solar-blind UV photodetectors [5], and as varistor material [6]. In all of these applications it is crucial to control the properties of electrical contacts.

The understanding of contact formation has improved significantly since the first systematic investigation by Mead on vacuum-cleaved single crystals [7]. Starting with the description of the importance of an excess monolayer of oxygen for the potential barrier height at ZnO varistor grain boundaries by Stucki and Greuter [8], many studies have shown the importance of oxygen and oxygen vacancies (V_O) for electrical contacts to ZnO. Using a remote oxygen plasma treatment prior to contact deposition, widely used Au contacts can be converted from ohmic to rectifying with barrier heights up to 0.5 eV [9]. Mosbacher *et al.* explained this with the plasma-induced reduction of adsorbates and reduction of the concentration of deep defects. With the addition of oxygen to the process gas during deposition of noble metal contacts, Allen *et al.* could improve the quality of ZnO Schottky contacts reaching barrier heights of up to 1.2 eV and ideality factors near 1 [10–12]. Oxidized noble metal contacts were also in the focus of more recent research, in which an improvement of barrier heights of Pt and Pd was reached by processing with oxygen [13,14].

One of the driving forces of recent research on ZnO has been the emerging field of piezotronics [2–4]. For such applications it is essential that Schottky barrier heights (SBHs)

at metal contacts depend on polarization, which would be manifested by different SBHs on the oxygen- and zinc-terminated surfaces of *c*-axis oriented ZnO and in a dependence of barrier height on strain. Studies of the polarization dependence of ZnO Schottky barrier heights have revealed either no significant difference or indicated higher barriers on zinc- as compared to oxygen-terminated surfaces [10,15–18]. However, the observed dependence of SBH on ZnO surface termination has not been related to the polarity of the surface, but to the different concentration of deep defects, usually oxygen vacancies (V_O), which are supposed to induce Fermi level pinning [9,16,19]. Therefore, in order to investigate the influence of polarization on SBH, one has to guarantee that no pinning of the Fermi level occurs. Such a pinning might also be introduced during metal electrode deposition itself. As an example, the SBHs of as-deposited Cu, Ag, and Pt on Pb(Zr, Ti)O₃ are almost identical despite strongly different metal work functions [20]. As this comes along with the observation of the formation of metallic Pb during deposition, it is reasonable to assign the pinning to the reduction of the substrate by metal deposition, which has also been discussed for other interfaces in the literature [21–27].

In this work we have investigated the chemical and electronic properties of ZnO/metal interfaces. Various ZnO substrates with different defect concentrations have been used. Furthermore, the influence of oxygen on interface properties has been assessed. High Schottky barriers of up to 1.5 eV are obtained by suppressing the chemical reduction of ZnO during metal deposition by processing with oxygen. A variation of the core hole screening during evolution of the barrier height is identified from a comparison of the binding energy shifts of the ZnO core levels and the Zn LMM Auger emission. Consequently, the barrier heights cannot be directly extracted from the core level binding energies but a correction for the

^{*}andreas.klein@tu-darmstadt.de

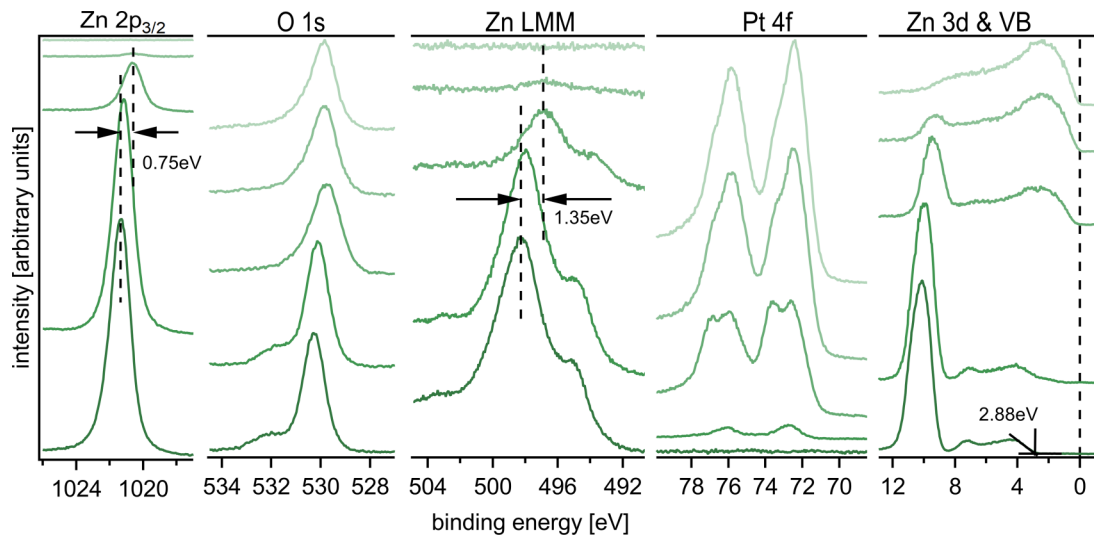


FIG. 1. XPS spectra recorded during deposition of PtO_x onto ZnO. The spectra at the bottom show the bare substrate, the following ones after deposition of 1, 2, 4, and 8 nm of PtO_x . Binding energy shifts of the Zn $2p_{3/2}$ core level and of the Zn LMM Auger line are indicated.

change of screening has to be applied. The corrected Schottky barrier heights at interfaces with metallic RuO_2 exhibit a substantial dependence on ZnO preparation, which is assigned to a different magnitude of Fermi level pinning by oxygen vacancies. In the absence of pinning, the SBHs of RuO_2 on c -axis oriented ZnO are ~ 240 meV higher on the oxygen-terminated surface as compared to the zinc-terminated surface.

II. EXPERIMENTAL

The interface formation has been studied using the Darmstadt Integrated System for MATerials research (DAISY-MAT [28]), which combines a multitechnique surface analysis system (Physical Electronics PHI 5700) and several thin film deposition chambers connected via an ultrahigh-vacuum (UHV) sample transfer. Interface formation is studied using stepwise deposition of a contact material onto freshly prepared or cleaned substrates and x-ray photoelectron spectroscopy (XPS) analysis after each preparation step [28]. Substrate preparation, contact layer deposition, and XPS analysis are all performed without breaking vacuum. The barrier heights are extracted from such measurements using core level binding energies and the energy difference between the core levels and the valence band maximum as proposed by Kraut and coworkers [29,30].

Thin films were deposited using magnetron sputtering at a chamber pressure of 0.5 Pa. For Pt and PtO_x a metallic Pt target of 2 inch diameter, DC plasma excitation with a power of 5 W, a gas flux of 6.6 sccm, and a target-to-substrate distance of 7.5 cm were used. The process gas was pure Ar and a 1 : 1 Ar : O_2 mixture for Pt and PtO_x , respectively. RuO_2 films were deposited from a metallic Ru target with a RF plasma excitation at 13.56 MHz and a power of 25 W. A gas flux of 10 sccm with 7.5% O_2 in Ar and a target-to-substrate distance of 10 cm have been used. All electrodes were deposited without intentional heating. ZnO thin films were deposited from ceramic ZnO targets using 25 W RF

excitation, a 10 cm target-to-substrate distance, and a total gas flux of 10 sccm with a gas composition of 3% O_2 and 97% Ar.

The (0001)-oriented ZnO single crystals were purchased from MaTecK (Jülich, Germany). After introducing the crystals into the UHV system they were cleaned by heating in 1 Pa O_2 atmosphere at 400 °C for two hours.

XPS spectra were recorded using monochromatic Al $K\alpha$ radiation with an energy resolution of around 0.4 eV. If not stated differently, the angle between the surface normal and the x-ray source and the detector were both 45°. Binding energies are measured with respect to the Fermi energy, which has been calibrated with a sputter-cleaned Ag foil.

III. RESULTS AND DISCUSSION

A. Interface reactivity

To evaluate the differences between metallic and oxidized Schottky contacts, interface experiments with Pt and PtO_x on polycrystalline ZnO films were performed. The XPS spectra recorded in the course of PtO_x deposition are shown in Fig. 1. Those recorded in the course of stepwise deposition of metallic Pt are shown in Fig. S1 in the Supplemental Material [31]. The valence band maximum (VBM) of ZnO before PtO_x deposition is determined as 2.88 eV below the Fermi energy. With increasing PtO_x thickness, the recorded Zn $2p_{3/2}$, Zn 3d, and Zn LMM emission lines are attenuated, the Pt 4f emission increases, and a Fermi edge emerges. The spectra confirm the growth of PtO_x and its metallic character [32]. Formation of a Schottky barrier is evident from the shift of the emissions to lower binding energy in the course of metal deposition.

Metallic Zn and ZnO can hardly be discriminated from the Zn $2p$ emission [33] but the Auger emission is more sensitive to changes in the oxidation state of Zn atoms [34]. This is due to competing effects of initial and final state contributions to core level binding energies [35,36]. Figure 2 shows the Zn LMM emission lines and difference spectra of ZnO thin films before and after deposition of 1 nm Pt (a) and of 1 nm PtO_x (b). The shapes of the Auger emission lines of the

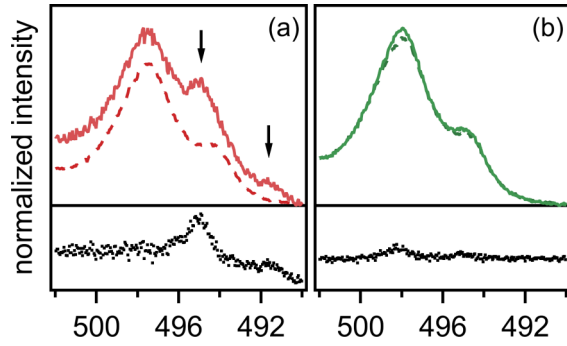


FIG. 2. Zn LMM Auger emission lines of the bare substrates (dashed lines) and after deposition of 1 nm of Pt (a) or of 1 nm PtO_x (b) (solid lines). The spectra have been normalized and shifted for better comparison and to calculate the difference (dots). The emissions at 495 eV and 492 eV in (a) indicate the formation of metallic Zn.

uncovered surfaces are the same, showing two main features at ~ 498 eV and ~ 495 eV. While there is no apparent change of the shape of the emission after deposition of PtO_x , two new features appear at 495 eV and 492 eV after deposition of metallic Pt. These new emissions are a signature of the formation of metallic Zn [34].

The evident reduction of ZnO by deposition of Pt is in line with a corresponding reduction of other oxides observed in the course of Pt deposition [26,27,37], which has been explained by the release of the heat of condensation of the deposited particles as originally suggested by Spicer and coworkers [23]. In agreement with previous reports [26,27,37], the reduction of ZnO pins the Fermi level, which is evident from the smaller binding energy shifts in the course of Pt deposition as compared to the deposition of PtO_x . This observation also agrees with a recent study of Schottky barrier formation of Pt on In_2O_3 [38], in which deposition of Pt results in very small barrier heights, regardless of substrate preparation. Postdeposition oxidation of the contact, which is also leading to the formation of PtO_x , results in a substantial increase of the SBH.

B. Determination of barrier heights

In order to determine the barrier height it is necessary to know the Fermi level position in the semiconductor's band gap before metal deposition and its change, ΔE_F , during contact formation. However, binding energy shifts in XPS are not only caused by chemical and surface potential changes. Hollinger summarized the factors by the following equation [39]:

$$\Delta E_B(\text{PE}) = \Delta\epsilon + \Delta E_F - \Delta R, \quad (1)$$

where $E_B(\text{PE})$ is the experimentally determined binding energy of the photoelectron, ϵ is the initial state energy describing the chemical state, and R is the final state energy describing intra- and extra-atomic relaxation effects. In the absence of charging effects and changes in chemical environment, the initial state energy remains constant ($\Delta\epsilon = 0$).

Relaxation affects the screening of the photoinduced core hole, which particularly alters the energy of Auger electrons, as their emission results in the presence of a doubly charged

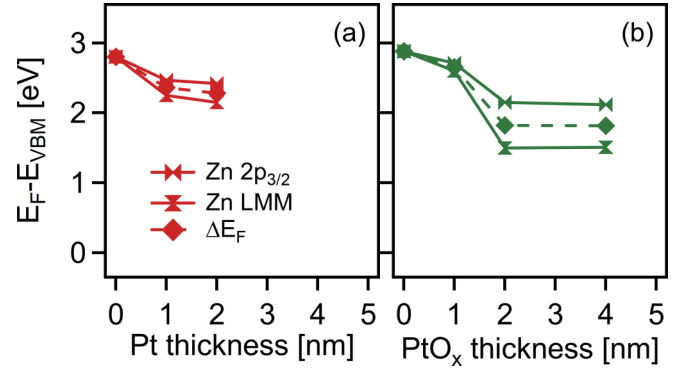


FIG. 3. Development of binding energies of the Zn $2p_{3/2}$ and the Zn LMM emissions during deposition of Pt (a) and PtO_x (b). The evolution of the Fermi energy at the interface as calculated using Eq. (3), which takes final state effects into account, is also shown.

final state. Therefore, ΔR can be extracted from the change of the Auger parameter, α' , which is defined as the sum of the photoelectron binding energy and the kinetic energy of the Auger electron:

$$\alpha' = E_B(\text{PE}) + E_{\text{kin}}(\text{AE}) = E_B(\text{PE}) + h\nu - E_B(\text{AE}). \quad (2)$$

Using the Auger parameter, the change in relaxation is given by $\Delta R = \frac{\Delta\alpha'}{2}$. Equation (1) can then be rewritten as

$$\Delta E_F = \frac{\Delta E_B(\text{PE}) + \Delta E_B(\text{AE})}{2}. \quad (3)$$

Auger emissions are rarely recorded in interface experiments as they often have low intensities. This is not an issue as long as the assumption $\Delta E_B(\text{AE}) \approx \Delta E_B(\text{PE})$ is valid. However, this is definitely not the case for the studied interfaces, which is evident from the significantly smaller binding energy shifts of the Zn $2p_{3/2}$ core level compared to the Zn LMM Auger line (see Fig. 1 and Fig. 3). It can be excluded that the different shifts are related to the different escape depths of the Zn $2p$ and Zn LMM electrons, which might occur if the extension of the space charge region is only a few nanometers [40,41]. In this case, the Zn LMM emission should shift less than the Zn $2p$. It is therefore concluded that ΔR substantially deviates from zero in the course of PtO_x deposition. In particular a reduction of the screening of the Zn $2p$ core hole occurs when the energy bands are bending upward at the surface during interface formation.

The origin of the reduction of the core hole screening is not clear. We have analyzed an extended set of XP spectra of ZnO films with different Fermi level positions. Except for degenerately Al-doped films with Fermi energies above the conduction band minimum, no significant changes of the Auger parameter could be identified. The deviation for degenerately doped films can be explained by the high electron concentration in the conduction band, which contributes an additional screening of the core hole [42]. A contribution of the high electron concentration in the deposited metal to screening of the Zn $2p$ core hole, equivalent to an image charge effect, is not likely. This is expected to improve screening, opposite to what is observed here. A potential origin of the reduced screening might be the electric field in the surface region, which is introduced by the barrier formation

due to the high work functions of the deposited oxides. The electric field will remove secondary electrons and electron-hole pairs from the surface space charge region. These carriers are generated during the photoemission process in inelastic scattering events and can result in substantial photovoltage shifts of the photoelectron spectra [27,43]. Systematic studies may confirm such a contribution.

The binding energies of the Zn $2p_{3/2}$ and the Zn LMM emissions during interface formation with Pt and PtO_x are depicted in Fig. 3 together with the calculated evolution of the Fermi energy at the interface using Eq. (3). The evaluation of the binding energies as a function of film thickness is limited by the Zn LMM Auger line intensity and possible up to ~ 4 nm for deposition of PtO_x and up to ~ 2 nm for deposition of Pt. The different attenuation of the Zn LMM intensity by PtO_x and Pt is assigned to the higher photoelectron inelastic mean free path in PtO_x due to its lower density [44].

According to Fig. 3, the distance between the Fermi level and the valence band maximum at the interfaces with Pt and PtO_x is determined as 2.28 eV and 1.81 eV above the valence band maximum, respectively. Taking the energy gap of ZnO at room temperature as 3.3 eV [1] one can calculate Schottky barrier heights of 1.52 eV for PtO_x and of 1.02 eV for Pt. The barrier heights are comparable with those obtained using electrical measurements, which revealed SBHs in the range of 1 to 1.3 eV for PtO_x and up to 0.9 eV for Pt contacts [12,13,16]. As electrical measurements are more sensitive to barrier inhomogeneities than XPS measurements [45], higher effective Schottky barrier heights obtained using photoelectron spectroscopy are to be expected.

C. Influence of polarization on barrier heights

The influence of polarization on SBH is studied for ZnO/RuO₂ interfaces, for which a more extensive data set is available. RuO₂ is also a high work function oxide and can exhibit comparable barrier heights to PtO_x .

A first study of the interface formation between RuO₂ and Zn- and O-terminated ZnO surfaces has been reported previously [17]. In this study, the cleaned single-crystal surfaces showed a substantially different Fermi level position with 3.15 eV and 2.85 eV for Zn and O termination, respectively. The difference has been assigned to the polarity of the ZnO surfaces being partially compensated by free electrons. In the course of RuO₂ deposition, the Fermi energy decreased to 2.5 eV for both surfaces, suggesting no influence of polarization on the Schottky barrier height. However, deposition of RuO₂ onto a ZnO thin film reported in the same publication revealed a significantly lower Fermi energy of 2.17 eV. This suggests that the SBHs of those single crystals are modified by Fermi level pinning. Indeed, the observed Fermi energies at the single-crystal interfaces of 2.5 eV above VBM correspond well with the charge transition level of the oxygen vacancy, which has been reported to be 0.7 to 0.8 eV below the conduction band minimum [11,46]. Such a pinning will be observed in XPS measurements, as the width of the space charge region becomes comparable to the inelastic mean path of the photoelectrons for high defect concentrations [41].

A series of experiments has been performed in this work to examine the influence of oxygen vacancies and of the

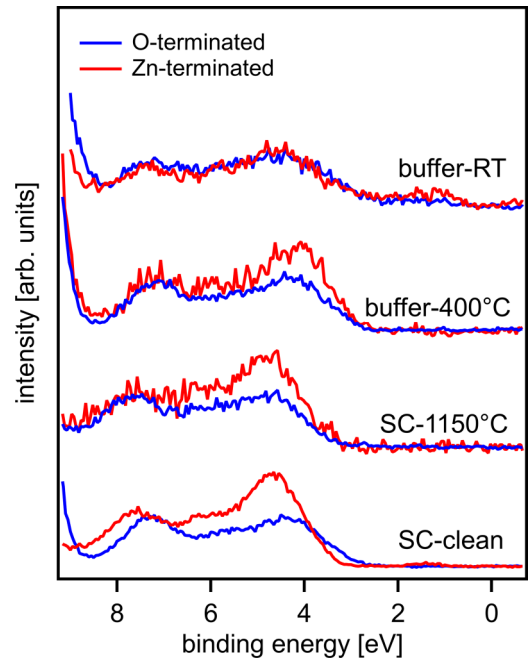


FIG. 4. XP valence band spectra of (i) *c*-axis oriented single crystal surfaces without high-temperature treatment after cleaning by heating at 400 °C, (ii) after high-temperature treatment without cleaning, (iii) after high-temperature treatment and subsequent deposition of a ZnO buffer layer at 400 °C, and (iv) after high-temperature treatment and subsequent deposition of a ZnO buffer layer at room temperature. The spectra were recorded with 10° take-off angle. The different shapes and intensities of the valence bands are characteristic for polar Zn- and O-terminated ZnO surfaces [48,49]. The difference vanishes for room temperature deposition of the buffer layer, indicating that no single polarity of the surface remains.

polarity of ZnO on the Schottky barrier height. ZnO single crystals with *c*-axis orientation with and without buffer layers have been used. Prior to buffer layer deposition, the crystals were annealed for one hour at 1150 °C in air according to the procedure suggested by Neumann for homoepitaxial ZnO growth [47]. Oxygen was added to the process gas during buffer layer deposition in order to reduce the oxygen vacancy concentration. In contrast to the earlier study, the Zn LMM Auger line was recorded during interface formation in order to reveal accurate shifts of the Fermi energy.

1. Surface termination

To verify the polarization of the surface, x-ray valence band spectra have been recorded with a take-off angle of 10° to confirm the termination of the wurtzite-type ZnO single crystals and of the ZnO thin film buffer layers following a procedure outlined in the literature [48,49]. The spectra are shown in Fig. 4. It is found that the polar termination is observed for the single crystals and conserved after buffer layer deposition at 400 °C. In contrast, no termination can be identified for buffer layer deposition at room temperature, despite the fact that magnetron-sputtered ZnO films typically grow with a strongly preferred *c*-axis orientation [1]. The absence of surface polarity at the room temperature buffer layer surfaces may hence be related to the formation of inversion

domain boundaries, which can reverse polarity and lead to mixed surface terminations of *c*-axis oriented films [50].

The XP valence band spectra recorded with a 45° take-off angle from the different Zn- and O-terminated surfaces are included in Figs. S2–S4 in the Supplemental Material [31]. The valence band spectra of the single-crystal surfaces without a buffer layer revealed Fermi levels of 3.00 eV and 3.14 eV above the valence band maximum for the Zn- and O-terminated surfaces, respectively. This difference is smaller than that observed in the previous experiment (see above and Ref. [17]).

Deposition of the 25 nm thick buffer layers lowers the Fermi energy to 2.86 eV and 2.84 eV for the deposition at 400 °C and to 2.46 eV and 2.43 eV for room temperature deposition, respectively. The lower Fermi energy after buffer layer deposition indicates an oxidation of the ZnO substrate, which should be accompanied by a reduction of oxygen vacancy concentration. A reduced influence of Fermi level pinning on the Schottky barrier height is therefore expected. The lowering of the Fermi energy is less pronounced if the buffer layer is deposited at 400 °C, which can be explained by the higher diffusivity of oxygen and zinc [51,52], resulting in a partial equilibration of the defect concentrations between the buffer layer and the single-crystal substrate.

There is no significant difference in Fermi energy between the Zn- and the O-terminated surfaces after buffer layer deposition. Different binding energies would be expected if the polarity of the surface were partially compensated by free electrons or holes. However, as long as details of the surface reconstructions, which can be quite complex for ZnO [53,54], are not known, it is not possible to assess a possible electronic compensation of the polarization at ZnO surfaces. Moreover, no studies resolving the atomic structure of O-terminated ZnO surfaces are available. In addition, adatoms can also strongly modify the surface termination and completely compensate polarization [55]. Due to the hydrophilicity of ZnO and its strong tendency to form hydroxides [56–58], the presence of adsorbates is very likely, even in an ultrahigh-vacuum environment. That different adsorbates are involved is evident from the O 1s spectra of the clean surfaces, which are shown in the Supplemental Material [31] (Fig. S5).

The surface reconstruction and adsorbate coverage are likely modified in the course of metal deposition. Moreover, the particular compensation of polarity at the surface is no longer required at the interface to the metal, at which the polarization can be compensated by interface charges in the metal. Therefore, it is believed that the uncertainty regarding the potential contribution of free surface charges to the compensation of surface polarity does not affect our conclusion regarding the influence of polarization on the Schottky barrier heights.

2. Interface characterization

The XP spectra recorded in the course of RuO₂ deposition onto the Zn- and O-terminated surfaces of ZnO single crystals without a buffer layer, with a room temperature ZnO buffer layer and with a ZnO buffer layer deposited at 400 °C, are shown in the Supplemental Material [31] in Figs. S2–S4. The evolution of the Fermi energy for the different interfaces,

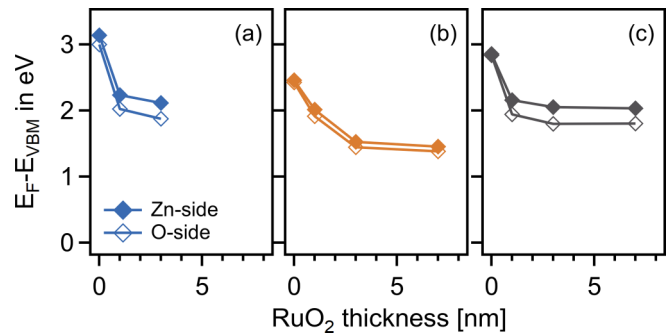


FIG. 5. Evolution of the Fermi energy in the ZnO band gap for RuO₂ deposition onto (a) ZnO single crystals, (b) ZnO single crystals with room temperature ZnO buffer layers, (c) ZnO single crystals with ZnO buffer layers deposited at 400 °C. The Fermi level shifts are calculated according to Eq. (3). The Zn LMM Auger emissions in (a) were only recorded up to 3 nm.

which is extracted from the binding energies of the Zn 2*p* core level and the Zn LMM Auger emission using Eq. (3), is shown in Fig. 5. In all cases, deposition of RuO₂ results in a downward shift of the Fermi energy by ~1 eV. The Fermi energies reached are much lower than those observed in our earlier study [17] and also significantly lower than the energy of the oxygen vacancy. This confirms that pinning by oxygen vacancies is not limiting the Fermi energy shifts in the present experiments.

For the bare single crystals and the high-temperature buffer layer samples, the Fermi energy reaches values that are ~240 meV higher at the Zn-terminated surfaces as compared to those at the O-terminated surfaces. For the room temperature buffer layer, which does not exhibit a unique surface polarity, the difference in Fermi energy is only 50 meV. Higher Fermi energies correspond to lower Schottky barrier heights for electrons. Consequently, we find higher SBH on O-terminated surfaces. All values, including calculated barrier heights and additional samples, are summarized in Table S1 in the Supplemental Material [31].

A clear difference in barrier height is observed for surfaces where the polarity is demonstrated by the XP valence spectra, whereas no difference is observed in the absence of a unique surface polarization. Therefore, we assign the different SBHs on the Zn- and the O-terminated surfaces to the polarization of ZnO. The absence of different barrier heights on Zn- and O-terminated surfaces in the earlier measurements [17] is likely caused by a high oxygen vacancy concentration induced Fermi level pinning.

The dependence of barrier height on polarization can be explained by an imperfect screening of the bound polarization charge of ZnO by the charge carriers in RuO₂ [59–61]. Such an imperfect screening is responsible for the so-called dead layers, which reduce the capacitance of thin dielectric films [62]. The difference between perfect and imperfect screening is schematically illustrated in Fig. 6.

An imperfect screening of the bound charges can be understood as a spatial separation between the bound surface charge of the polar material and the screening charge in the metal. This results in a potential drop across the dead layer, which cannot be detected by XPS as the effective screening length

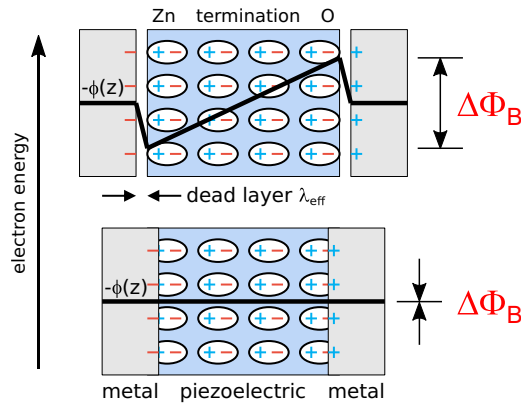


FIG. 6. Representation of changes in the electrostatic potential of a polar oxide with imperfect screening (top) and perfect screening (bottom) of the polarization charge as proposed by Stengel *et al.* [61]. An imperfect screening is equivalent to a spatial separation of the bound surface charge of the polar material and the screening charge in the metal. Imperfect screening results in a potential drop across the dead layer. XPS will probe the potential below the dead layer, as this extends only about an atomic bond length, which is much thinner than the information depth of XPS.

λ_{eff} is typically shorter than 1 \AA [61], much thinner than the information depth of XPS. The presence of such layers and its influence on the effective Schottky barrier heights have been observed previously by XPS using ferroelectric materials with electrically switchable polarization [63–66].

The screening of the polarization charge depends on the atomic configuration at the interface and may therefore vary from interface to interface [60]. There are even situations where an enhancement of polarization may occur, corresponding to a negative effective screening length [60]. For other ZnO/metal interfaces, the dependence of barrier height on polarization will therefore likely be different from what is observed here. The polarization dependence itself is also influenced by the quality of the interface, which will be affected by the details of interface preparation [66].

Consequently, the polarization dependence of ZnO Schottky barrier heights cannot be predicted quantitatively. It depends on the choice of contact material and on interface preparation. However, it is evident that it is essential to exclude effects of Fermi level pinning to reveal the dependence of barrier height on polarization. The influence of defects may even lead to a dependence that is opposite to what is observed in this study (compare Fig. 5) [10,11,16,67]. If pinning effects

can be excluded, the dependence of SBH on polarization should follow the behavior known for ferroelectric materials, where imperfect screening is required for an influence of polarization on SBH.

IV. SUMMARY AND CONCLUSIONS

The formation of Schottky barriers of high work function metals on ZnO has been studied. Using photoelectron spectroscopy it could be demonstrated that the low electron Schottky barrier heights on ZnO observed with high work function metals are caused by the chemical reduction of the substrate. The reduction is induced by the condensation energy of the metal atoms and can be overcome by processing with oxygen.

By analysis of the Zn LMM Auger emissions, it has been further demonstrated that the screening of the photoelectron core holes is reduced in the course of barrier formation. This affects the conventional extraction of Fermi level positions during interface experiments using core level binding energies in photoelectron spectroscopy and results in corrections of derived Schottky barriers by up to 215 meV in our experiments. The correction requires simultaneous recording of a core level and a related Auger emission. The origin of the reduced screening remains unclear. It might be related to the electric field, which is generated near the ZnO surface due to the formation of a high Schottky barrier.

Fermi level pinning at ZnO Schottky barriers by oxygen vacancies can be avoided by suitable preparation conditions of the substrates and by deposition of metallic oxide contact materials using reactive magnetron sputtering. Avoiding such a pinning, a dependence of Schottky barrier height on the polarity of the c -axis oriented ZnO surfaces could be revealed. For RuO_2 contacts on polar surfaces, the Schottky barriers on the oxygen-terminated surfaces are ~ 240 meV higher than on the zinc-terminated surfaces. This indicates that the Schottky barriers can depend on surface termination, if the ZnO surface polarity is incompletely screened by the metal electrode. The dependence of barrier height on polarization is expected to be different for different contact materials and interface preparation.

ACKNOWLEDGMENTS

The presented work has been supported by the German Science Foundation (DFG), Project No. KL1225/8-1, and by the European Union’s Horizon 2020 research and innovation program under Marie Skłodowska-Curie Grant Agreement No. 641640 (EJD-ITN project FunMAT).

- [1] K. Ellmer, A. Klein, and B. Rech (Eds.), *Transparent Conductive Zinc Oxide* (Springer, Berlin, 2008).
- [2] Z. L. Wang, Progress in piezotronics and piezo-phototronics, *Adv. Mater.* **24**, 4632 (2012).
- [3] R. Zhang, M. Hummelgård, M. Olsen, J. Örtengren, and H. Olin, Nanogenerator made of ZnO nanosheet networks, *Semicond. Sci. Technol.* **32**, 054002 (2017).

- [4] J. Zhou, Y. Gu, P. Fei, W. Mai, Y. Gao, R. Yang, G. Bao, and Z. L. Wang, Flexible piezotronic strain sensor, *Nano Lett.* **8**, 3035 (2008).
- [5] R. Khokhra, B. Bharti, H.-N. Lee, and R. Kumar, Visible and UV photo-detection in ZnO nanostructured thin films via simple tuning of solution method, *Sci. Rep.* **7**, 15032 (2017).

- [6] D. R. Clarke, Varistor ceramics, *J. Am. Ceram. Soc.* **82**, 485 (1999).
- [7] C. A. Mead, Metal-semiconductor surface barriers, *Solid State Electron.* **9**, 1023 (1966).
- [8] F. Stucki and F. Greuter, Key role of oxygen at zinc oxide varistor grain boundaries, *Appl. Phys. Lett.* **57**, 446 (1990).
- [9] H. L. Mosbacker, Y. M. Strzhemechny, B. D. White, P. E. Smith, D. C. Look, D. C. Reynolds, C. W. Litton, and L. J. Brillson, Role of near-surface states in ohmic-Schottky conversion of Au contacts to ZnO, *Appl. Phys. Lett.* **87**, 012102 (2005).
- [10] M. W. Allen, S. M. Durbin, and J. B. Metson, Silver oxide Schottky contacts on *n*-type ZnO, *Appl. Phys. Lett.* **91**, 053512 (2007).
- [11] M. W. Allen and S. M. Durbin, Influence of oxygen vacancies on Schottky contacts to ZnO, *Appl. Phys. Lett.* **92**, 122110 (2008).
- [12] M. W. Allen, R. J. Mendelsberg, R. J. Reeves, and S. M. Durbin, Oxidized noble metal Schottky contacts to *n*-type ZnO, *Appl. Phys. Lett.* **94**, 103508 (2009).
- [13] A. M. Hyland, R. A. Makin, S. M. Durbin, and M. W. Allen, Giant improvement in the rectifying performance of oxidized Schottky contacts to ZnO, *J. Appl. Phys.* **121**, 024501 (2017).
- [14] T. Schultz, S. Vogt, P. Schlupp, H. von Wenckstern, N. Koch, and M. Grundmann, Influence of Oxygen Deficiency on the Rectifying Behavior of Transparent-Semiconducting-Oxide-Metal Interfaces, *Phys. Rev. Appl.* **9**, 064001 (2018).
- [15] Y. Dong, Z. Q. Fang, D. C. Look, G. Cantwell, J. Zhang, J. J. Song, and L. J. Brillson, Zn- and O-face polarity effects at ZnO surfaces and metal interfaces, *Appl. Phys. Lett.* **93**, 072111 (2008).
- [16] L. J. Brillson and Y. Lu, ZnO Schottky barriers and Ohmic contacts, *J. Appl. Phys.* **109**, 121301 (2011).
- [17] M. T. Uddin, Y. Nicolas, T. Toupance, S. Li, A. Klein, and W. Jaegermann, Improved photocatalytic activity in RuO₂-ZnO nanoparticulate heterostructures due to inhomogeneous space charge effects, *Phys. Chem. Chem. Phys.* **17**, 5090 (2015).
- [18] P. Keil, T. Frömling, A. Klein, J. Rödel, and N. Novak, Piezotronic effect at Schottky barrier of a metal-ZnO single crystal interface, *J. Appl. Phys.* **121**, 155701 (2017).
- [19] L. J. Brillson, H. L. Mosbacker, M. J. Hetzer, Y. Strzhemechny, G. H. Jessen, D. C. Look, G. Cantwell, J. Zhang, and J. J. Song, Dominant effect of near-interface native point defects on ZnO Schottky barriers, *Appl. Phys. Lett.* **90**, 102116 (2007).
- [20] F. Chen, R. Schafrank, W. Wu, and A. Klein, Reduction induced Fermi level pinning at the interfaces between Pb(Zr,Ti)O₃ and Pt, Cu, and Ag metal electrodes, *J. Phys. D: Appl. Phys.* **44**, 255301 (2011).
- [21] L. J. Brillson, Transition in Schottky Barrier Formation with Chemical Reactivity, *Phys. Rev. Lett.* **40**, 260 (1978).
- [22] W. Walukiewicz, Mechanism of Fermi-level stabilization in semiconductors, *Phys. Rev. B* **37**, 4760 (1988).
- [23] W. E. Spicer, P. W. Chye, P. R. Skeath, C. Y. Su, and I. Lindau, New and unified model for Schottky barrier and III-V insulator interface states formation, *J. Vac. Sci. Technol.* **16**, 1422 (1979).
- [24] A. Klein, C. Pettenkofer, W. Jaegermann, T. Chassé, K. Horn, M. Ch. Lux-Steiner, and E. Bucher, Interface reaction of Pt on p-WSe₂(0001) surfaces, *Surf. Sci. Lett.* **264**, 193 (1992).
- [25] P. Hanys, P. Janecek, V. Matolin, G. Korotcenkov, and V. Nehasil, XPS and TPD study of Rh/SnO₂ system: Reversible process of substrate oxidation and reduction, *Surf. Sci.* **600**, 4233 (2006).
- [26] C. Körber, S. P. Harvey, T. O. Mason, and A. Klein, Barrier heights at the SnO₂/Pt interface: *In situ* photoemission and electrical properties, *Surf. Sci.* **602**, 3246 (2008).
- [27] R. Schafrank, S. Payan, M. Maglione, and A. Klein, Barrier heights at (Ba, Sr)TiO₃/Pt interfaces studied by photoemission, *Phys. Rev. B* **77**, 195310 (2008).
- [28] A. Klein, Energy band alignment at interfaces of semiconducting oxides: A review of experimental determination using photoelectron spectroscopy and comparison with theoretical predictions by the electron affinity rule, charge neutrality levels, and the common anion, *Thin Solid Films* **520**, 3721 (2012).
- [29] E. A. Kraut, R. W. Grant, J. R. Waldrop, and S. P. Kowalczyk, Precise Determination of the Valence-Band Edge in X-Ray Photoemission Spectra: Application to Measurement of Semiconductor Interface Potentials, *Phys. Rev. Lett.* **44**, 1620 (1980).
- [30] J. R. Waldrop, R. W. Grant, S. P. Kowalczyk, and E. A. Kraut, Measurement of semiconductor heterojunction band discontinuities by x-ray photoemission spectroscopy, *J. Vac. Sci. Technol. A* **3**, 835 (1985).
- [31] See Supplemental Material at <http://link.aps.org/supplemental/10.1103/PhysRevMaterials.4.084604> for photoelectron spectra recorded during interface formation between ZnO and Pt and between different ZnO substrates and RuO₂, for O 1s spectra of clean ZnO surfaces and for a summary of studied samples and extracted energies.
- [32] V. Johánek, M. Václavů, I. Matolínová, I. Khalakhan, S. Haviar, and V. Matolín, High low-temperature CO oxidation activity of platinum oxide prepared by magnetron sputtering, *Appl. Surf. Sci.* **345**, 319 (2015).
- [33] C. J. Powell and A. Jablonski, *NIST Electron Inelastic-Mean-Free-Path Database*, Version 1.2 (National Institute of Standards and Technology, Gaithersburg, MD, 2010).
- [34] G. E. Hammer and R. M. Shemanski, The oxidation of zinc in air studied by XPS and AES, *J. Vac. Sci. Technol. A* **1**, 1026 (1983).
- [35] N. Rössler and V. Staemmler, *Ab initio* calculations for the 2s and 2p core level binding energies of atomic Zn, Zn metal, and Zn containing molecules, *Phys. Chem. Chem. Phys.* **5**, 3580 (2003).
- [36] N. Rössler, K. Kotsis, and V. Staemmler, *Ab initio* calculations for the Zn 2s and 2p core level binding energies in Zn oxo compounds and ZnO, *Phys. Chem. Chem. Phys.* **8**, 697 (2006).
- [37] F. Chen, R. Schafrank, W. Wu, and A. Klein, Formation and modification of Schottky barriers at the PZT/Pt Interface, *J. Phys. D: Appl. Phys.* **42**, 215302 (2009).
- [38] J. Michel, D. Splith, J. Rombach, A. Papadogianni, T. Berthold, S. Krischok, M. Grundmann, O. Bierwagen, H. von Wenckstern, and M. Himmerlich, Processing strategies for high-performance Schottky contacts on *n*-type oxide semiconductors: Insights from In₂O₃, *ACS Appl. Mater. Interfaces* **11**, 27073 (2019).
- [39] G. Hollinger, Structures chimique et électronique de l'interface SiO₂-Si, *Appl. Surf. Sci.* **8**, 318 (1981).
- [40] N. Ohashi, H. Yoshikawa, Y. Yamashita, S. Ueda, J. Li, H. Okushi, K. Kobayashi, and H. Haneda, Determination of Schottky barrier profile at Pt/SrTiO₃: Nb junction by x-ray photoemission, *Appl. Phys. Lett.* **101**, 251911 (2012).

- [41] R. Giesecke, R. Hertwig, T. Bayer, C. A. Randall, and A. Klein, Modification of the cathodic Schottky barrier height at the RuO₂ cathode during resistance degradation of Fe-doped SrTiO₃, *J. Am. Ceram. Soc.* **100**, 4590 (2017).
- [42] R. G. Egdell, J. Rebane, T. J. Walker, and D. S. L. Law, Competition between initial- and final-state effects in valence- and core-level x-ray photoemission of Sb-doped SnO₂, *Phys. Rev. B* **59**, 1792 (1999).
- [43] M. H. Hecht, Role of photocurrent in low-temperature photoemission studies of Schottky barrier formation, *Phys. Rev. B* **41**, 7918 (1990).
- [44] S. Tanuma, C. J. Powell, and D. R. Penn, Calculations of electron mean free path. II: Data for 27 elements over the 50–2000 eV range, *Surf. Interface Anal.* **17**, 911 (1991).
- [45] R. T. Tung, Electron transport at metal-semiconductor interfaces: General theory, *Phys. Rev. B* **45**, 13509 (1992).
- [46] P. Ágoston, K. Albe, R. M. Nieminen, and M. J. Puska, Intrinsic *n*-Type Behavior in Transparent Conducting Oxides: A Comparative Hybrid-Functional Study of In₂O₃, SnO₂, and ZnO, *Phys. Rev. Lett.* **103**, 245501 (2009).
- [47] C. Neumann, S. Lautenschläger, S. Graubner, N. Volbers, B. K. Meyer, J. Bläsing, and A. Krost, Surface preparation of single crystals for ZnO homoepitaxy, *MRS Proc.* **957**, 0957-K07-31 (2006).
- [48] N. Ohashi, Y. Adachi, T. Ohsawa, K. Matsumoto, I. Sakaguchi, H. Haneda, S. Ueda, H. Yoshikawa, and K. Kobayashi, Polarity-dependent photoemission spectra of wurtzite-type zinc oxide, *Appl. Phys. Lett.* **94**, 122102 (2009).
- [49] J. Williams, H. Yoshikawa, S. Ueda, Y. Yamashita, K. Kobayashi, Y. Adachi, H. Haneda, T. Ohgaki, H. Miyazaki, T. Ishigaki, and N. Ohashi, Polarity-dependent photoemission spectra of wurtzite-type zinc oxide, *Appl. Phys. Lett.* **100**, 051902 (2012).
- [50] J. Hüpkes, J. I. Owen, S. E. Pust, and E. Bunte, Chemical etching of zinc oxide for thin-film silicon solar cells, *ChemPhysChem* **13**, 66 (2012).
- [51] P. Erhart and K. Albe, First-principles study of migration mechanisms and diffusion of oxygen in zinc oxide, *Phys. Rev. B* **73**, 115207 (2006).
- [52] P. Erhart and K. Albe, Diffusion of zinc vacancies and interstitials in zinc oxide, *Appl. Phys. Lett.* **88**, 201918 (2006).
- [53] O. Dulub, L. A. Boatner, and U. Diebold, STM study of the geometric and electronic structure of ZnO(0001)-Zn, (0001)-O, (10-10), and (11-20) surfaces, *Surf. Sci.* **519**, 201 (2002).
- [54] O. Dulub, U. Diebold, and G. Kresse, Novel Stabilization Mechanism on Polar Surfaces: ZnO(0001)-Zn, *Phys. Rev. Lett.* **90**, 016102 (2003).
- [55] K. Garrity, A. M. Kolpak, S. Ismail-Beigi, and E. I. Altman, Chemistry of ferroelectric surfaces, *Adv. Mater.* **22**, 2969 (2010).
- [56] V. Staemmler, K. Fink, B. Meyer, D. Marx, M. Kunat, S. G. Girol, U. Burghaus, and C. Wöll, Stabilization of Polar ZnO Surfaces: Validating Microscopic Models by Using CO as a Probe Molecule, *Phys. Rev. Lett.* **90**, 106102 (2003).
- [57] M. Kunat, S. G. Girol, U. Burghaus, and C. Wöll, The interaction of water with the oxygen-terminated, polar surface of ZnO, *J. Phys. Chem. B* **107**, 14350 (2003).
- [58] C. Wöll, The chemistry and physics of zinc oxide surfaces, *Prog. Surf. Sci.* **82**, 55 (2007).
- [59] M. Stengel and N. A. Spaldin, Origin of the dielectric dead layer in nanoscale capacitors, *Nature (London)* **443**, 679 (2006).
- [60] M. Stengel, D. Vanderbilt, and N. A. Spaldin, Enhancement of ferroelectricity at metal-oxide interfaces, *Nat. Mater.* **8**, 392 (2009).
- [61] M. Stengel, P. Aguado-Puente, N. A. Spaldin, and J. Junquera, Band alignment at metal/ferroelectric interfaces: Insights and artifacts from first principles, *Phys. Rev. B* **83**, 235112 (2011).
- [62] C. A. Mead, Anomalous Capacitance of Thin Dielectric Structures, *Phys. Rev. Lett.* **6**, 545 (1961).
- [63] F. Chen and A. Klein, Polarization dependence of Schottky barrier heights at interfaces of ferroelectrics determined by photoelectron spectroscopy, *Phys. Rev. B* **86**, 094105 (2012).
- [64] J. E. Rault, G. Agnus, T. Maroutian, V. Pillard, P. Lecoœur, G. Niu, B. Vilquin, M. G. Silly, A. Bendounan, F. Sirotti, and N. Barrett, Interface electronic structure in a metal/ferroelectric heterostructure under applied bias, *Phys. Rev. B* **87**, 155146 (2013).
- [65] E. Kröger, A. Petraru, A. Quer, R. Soni, M. Kalläne, N. A. Pertsev, H. Kohlstedt, and K. Rossnagel, *In situ* hard x-ray photoemission spectroscopy of barrier-height control at metal/PMN-PT interfaces, *Phys. Rev. B* **93**, 235415 (2016).
- [66] A. H. Hubmann, S. Li, S. Zhukov, H. von Seggern, and A. Klein, Polarisation dependence of Schottky barrier heights at ferroelectric BaTiO₃/RuO₂ interfaces: Influence of substrate orientation and quality, *J. Phys. D: Appl. Phys.* **49**, 295304 (2016).
- [67] M. W. Allen, M. M. Alkaisi, and S. M. Durbin, Metal Schottky diodes on Zn-polar and O-polar bulk ZnO, *Appl. Phys. Lett.* **89**, 103520 (2006).